Layer-by-Layer Assembly of Clay-Carbon Nanotube Hybrid Superstructures

Chalmpes, Nikolaos; Kouloumpis, Antonios; Zygouri, Panagiota; Karouta, Niki; Spyrou, Konstantinos; Stathi, Panagiota; Tsoufis, Theodoros; Georgakilas, Vasilios; Gournis, Dimitrios; Rudolf, Petra

Published in:
ACS Omega

DOI:
10.1021/acsomega.9b01970

Publication date:
2019

ACS OMEGA

Article

Cite This: ACS Omega 2019, 4, 18100−18107

http://pubs.acs.org/journal/acsodf

Layer-by-Layer Assembly of Clay−Carbon Nanotube Hybrid Superstructures

Nikolaos Chalmpes,[†,∥] Antonios Kouloumpis,[*,†,‡,∥] Panagiota Zygouri,[†] Niki Karouta,[†] Konstantinos Spyrou,[†,‡] Panagiota Stathi,[‡,⊥] Theodoros Tsoufis,[‡,#] Vasilios Georgakilas,[§] Dimitrios Gournis,[*,†] and Petra Rudolf[*,‡]

[†]Department of Materials Science and Engineering, University of Ioannina, GR-45110 Ioannina, Greece

[‡]Zernike Institute for Advanced Materials, University of Groningen, Nijenborgh 4, NL-9747AG Groningen, The Netherlands

[§]Department of Materials Science, University of Patras, GR-26504 Patras, Greece

ABSTRACT: Much of the research effort concerning layered materials is directed toward their use as building blocks for the development of hybrid nanostructures with well-defined dimensions and behavior. Here, we report the fabrication through layer-by-layer deposition and intercalation chemistry of a new type of clay-based hybrid film, where functionalized carbon nanotubes are sandwiched between nanometer-sized smectite clay platelets. Single-walled carbon nanotubes (SWCNTs) were covalently functionalized in a single step with phenol groups, via 1,3-dipolar cycloaddition, to allow for stable dispersion in polar solvents. For the production of hybrid thin films, a bottom-up approach combining self-assembly with Langmuir−Schaefer deposition was applied. Smectite clay nanoplatelets act as a structure-directing interface and reaction media for grafting functionalized carbon nanotubes in a bidimensional array, allowing for a controllable layer-by-layer growth at a nanoscale. Hybrid clay/SWCNT multilayer films deposited on various substrates were characterized by X-ray reflectivity, Raman, and X-ray photoelectron spectroscopies, as well as atomic force microscopy.

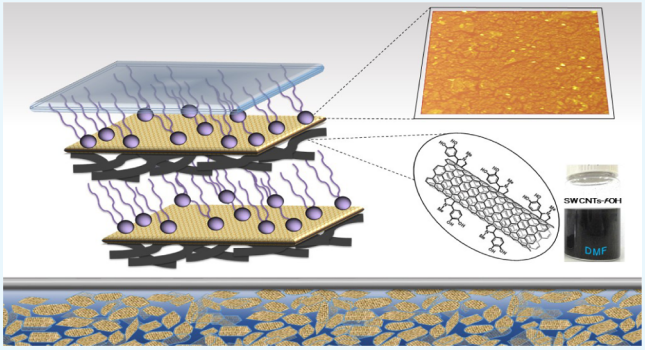

INTRODUCTION

Over the last decades, the industrial and scientific interest in layered materials has been mainly driven by their physical and chemical properties, resulting from the reduced dimensionality of the individual layers. Their structural characteristics and in particular their high surface area, combined with their unique (opto)electronic properties, render layered materials ideal for a wide range of applications in electronics,[1] nanosensing,[2] gas separations,[3] and energy storage,[4] as well as in biomedical technology and drug delivery.[5,6]

Layered aluminosilicate minerals (smectite clays) consisting of platelets, where an aluminum oxide octahedral sheet is sandwiched between two silicon oxide tetrahedral sheets, belong to the phyllosilicate family and exhibit a unique combination of properties including the ability to swell when put in contact with water, to adsorb molecules and organic/inorganic cationic moieties from solutions and to exchange cations located between the platelets.[7,8] The cation storage ability renders clay minerals an excellent template for embedding molecules and nanomaterials and forms the basis for the development of hybrids and nanocomposites with well-defined dimensions and behavior.[7]

On the other hand, carbon nanotubes (CNTs) are unique in their aspect ratio, mechanical strength, and electrical and thermal conductivities; therefore, they are an ideal nanomaterial for light-emitting diodes, smart windows, solar cells, nanofillers, self-healing thermoset/CNT nanocomposites, etc.[9−11] The integration of CNTs within two-dimensional (2D) materials (such as graphene and MoS_2) generates hybrid superstructures with improved mechanical stability and enhanced thermal and electrical properties due to the synergistic effects of 2D and one-dimensional materials.[12−15] Thus, the synthesis of hybrid nanomaterials, combining the properties of carbon nanotubes and layered materials with high surface area, has great potential for applications in the fields of catalysis,[16,17] sensing,[12,16,18] optoelectronics,[15,19] and biomedicine.[16,20]

Studies reported so far on the development of clay−CNT hybrid superstructures concern mainly their use as additives to increase the mechanical properties of polypropylene[21] and epoxy resin,[22,23] as well as in styrene−butadiene rubber nanocomposites[24] and as additives in Nafion polymer matrixes for electrolyte nanocomposite membranes.[25] In addition, clay−CNT hybrids reduce significantly the electrical percolation

Received: June 30, 2019
Accepted: September 27, 2019
Published: October 23, 2019

DOI: 10.1021/acsomega.9b01970
ACS Omega 2019, 4, 18100−18107

Scheme 1. Schematic Representation of the Synthetic Procedure Followed for the Development of the Hybrid DODA−Clay/SWCNTs-f-OH Multilayer Film

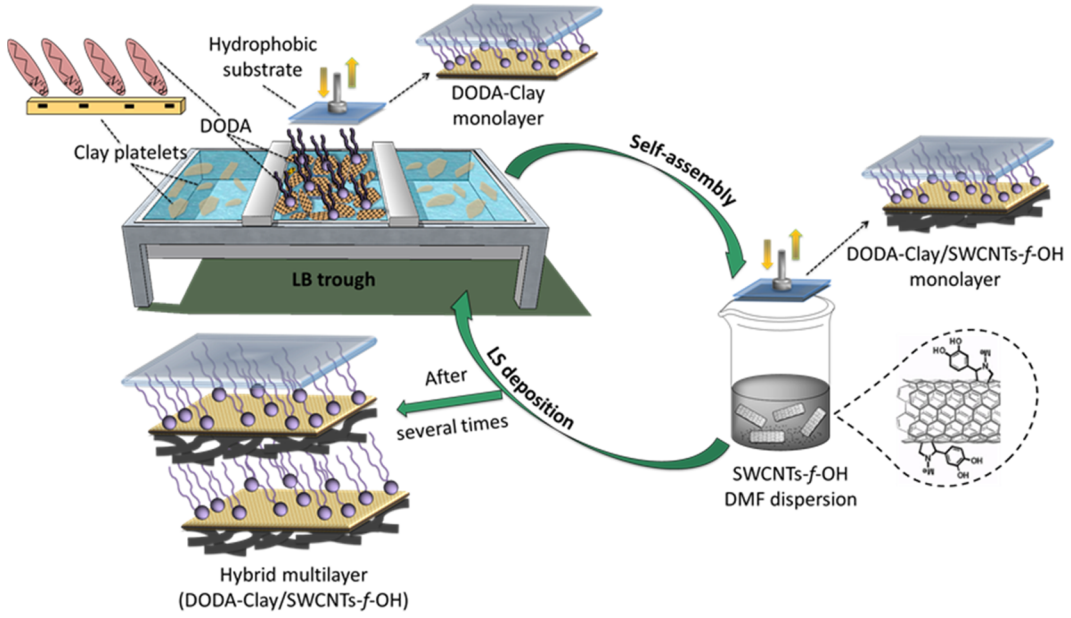

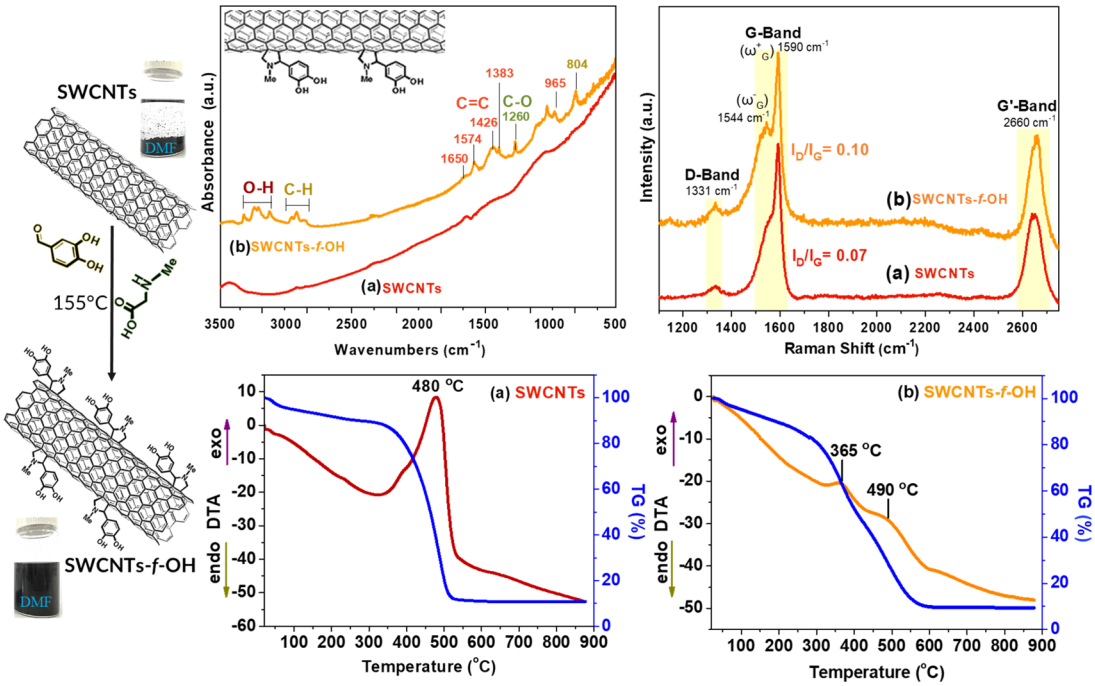

Figure 1. (Left) Schematic representation of SWCNT functionalization via 1,3-dipolar cycloaddition and photographs of suspensions of the two types of SWCNTs in DMF. (Top) FT-IR (center) and Raman (right) spectra of pristine SWCNTs (a) and SWCNTs-f-OH (b). (Bottom) Differential thermal analysis/thermogravimetric (DTA/TG) curves of pristine SWCNTs (a) and SWCNTs-f-OH (b).

threshold[26] and improve the electrical conductivity when incorporated in polypropylene and epoxy matrixes.[27] Moreover, due to the synergistic effect of clay nanoplatelets and carbon nanotubes, these hybrid structures have been proposed as flame retardants in unsaturated polyester resins and poly(methyl methacrylate)[28,29] as well as adsorbents for the removal of bacterial contaminants from different water supplies.[30]

In this work, we propose a simple and low-cost method for the development of hybrid clay multilayers accommodating functionalized single-walled carbon nanotubes (SWCNTs) based on the combination of Langmuir−Schaefer (LS) deposition and self-assembly.[31−33] SWCNTs, functionalized with phenol groups by 1,3-dipolar cycloaddition (SWCNTs-f-OH), were sandwiched between natural nanometer-sized clay platelets through layer-by-layer deposition to yield novel pillared structures with structural control at the molecular scale. An amino surfactant (dimethyldioctadecylammonium (DODA) bromide, $[CH_3(CH_2)_{17}]_2(CH_3)_2N^+Br^-$) was injected on top of an aqueous suspension of Na-montmorillonite (Kunipia-F) in the Langmuir−Blodgett trough to induce the formation of a hybridized Langmuir film at the air-suspension

DOI: 10.1021/acsomega.9b01970
ACS Omega 2019, 4, 18100−18107

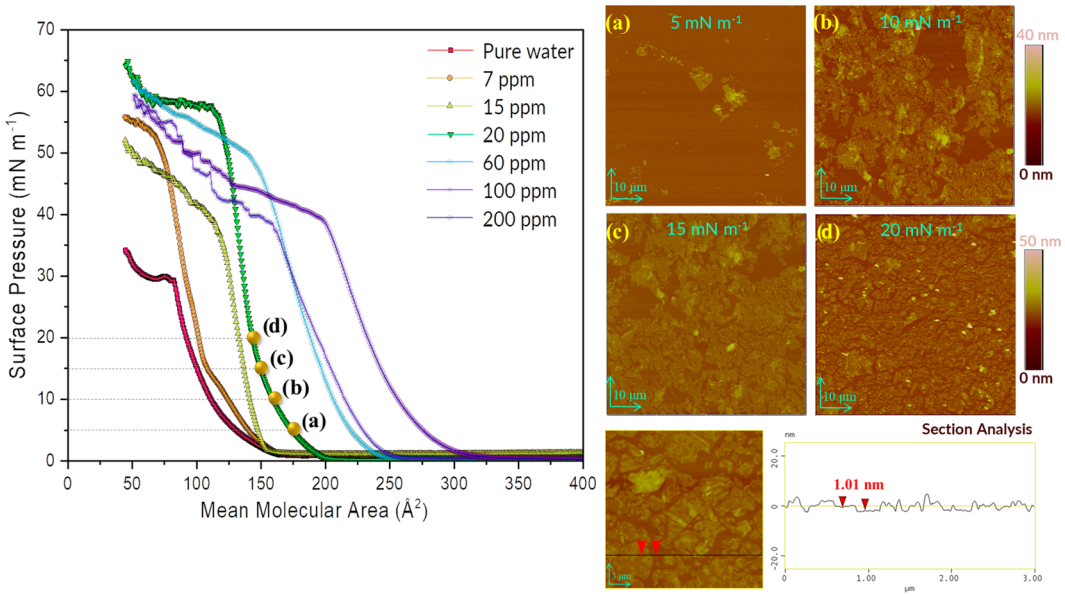

Figure 2. (Left) Π−*A* isotherms of DODA Langmuir films on pure water and on Kunipia aqueous suspensions. (Right) Atomic force microscopy (AFM) height images and cross-sectional analysis of DODA−clay monolayers deposited with the LS technique onto Si wafers at surface pressures of (a) 5 mN m^{-1}, (b) 10 mN m^{-1}, (c) 15 mN m^{-1}, and (d) 20 mN m^{-1} during the compression process.

interface. After the transfer of the compressed Langmuir film by horizontal dipping (Langmuir−Schaefer method), the substrate was immersed in a dispersion of SWCNTs-f-OH to prompt self-assembly. Hybrid multilayer films hosting SWCNTs within the interlayer space between clay platelets were fabricated by repeating this cycle for numerous times (Scheme 1) with the help of a robotic arm. These novel clay-based hybrid films could be excellent candidate nanomaterials for potential application as electrical conductivity improvers,[34,35] mechanical properties reformers,[21,22] nanoadditives in direct methanol fuel cells, or even as contaminant removal nanomaterial.[25] Moreover, when dispersed in a polymer matrix, clay−CNT additives create thermoprotection layers for electronics and enhance the proton conductivity.[36] Carbon nanotubes attached to smectite layers are also particularly attractive for polymer reinforcement[37,38] and the high surface area of these hybrid nanomaterials can be exploited for the removal of bacterial contaminants from different water supplies.[39]

RESULTS AND DISCUSSION

Structural and Morphological Characterization of SWCNTs-f-OH. The Fourier transform infrared (FT-IR) spectra of pristine SWCNTs and functionalized SWCNTs-f-OH are shown in Figure 1 (top center panel). In contrast to pristine SWCNTs, which are infrared inactive, additional vibrations are observed in the SWCNTs-f-OH spectrum. In more detail, C−H stretching bands appear at 804 cm^{-1} and between 3000 and 2800 cm^{-1}; C=C stretching bands are observed around 1600−1380 cm^{-1}, while the bands located at 1260 and 3320 cm^{-1} are attributed to the C−O and O−H stretching modes. Together, these vibrational fingerprints testify to the successful functionalization of SWCNTs with phenols. As a result of the covalent sidewall functionalization[9,40,41] with hydroxyl groups, the dispersibility of SWCNTs-f-OH in polar solvents is higher compared to that of pristine SWCNTs as observed in the photographs shown in Figure 1 (left panels).[9]

Raman spectra of SWCNTs-f-OH and pristine SWCNTs are shown in Figure 1 (top right panel). For both materials, the defect-induced D band appears at 1335 cm^{-1} and the G band splits into two modes, ω_G^- at 1545 cm^{-1} and ω_G^+ at 1590 cm^{-1}, resulting from the characteristic confinement and curvature of carbon nanotubes.[42−49] The I_D/I_G ratio of pristine SWCNTs and SWCNTs-f-OH was calculated to amount to 0.07 and 0.10, respectively. The slightly higher value for SWCNTs-f-OH agrees with the change in hybridization resulting from the covalent attachment of phenol moieties to the sidewall of nanotubes; however, the I_D/I_G of SWCNTs-f-OH is very low as expected for a high-quality graphitic structure.[9,41]

The differential thermal and thermogravimetric analyses of SWCNTs before and after functionalization are shown in Figure 1 (bottom center and bottom right panels). In the case of pristine nanotubes, one sharp exothermic peak at 480 °C is observed, followed by the complete decomposition of the graphitic lattice, while for SWCNTs-f-OH, two main exothermic peaks are seen. The first peak at 365 °C is attributed to the removal of aliphatic groups and the corresponding weight loss is estimated to be ∼33 wt %, while the second peak at 490 °C corresponds to the thermal decomposition of the graphitic network with a mass loss of ∼51 wt %. These results provide further evidence for the successful covalent functionalization of the SWCNTs.

Structural Control and Characterization of Hybrid DODA−Clay/SWCNTs-f-OH Monolayers. ∏−*A* isotherms of DODA monolayers on pure water and on the Kunipia suspension were recorded during the compression of the Langmuir films and are shown in Figure 2. The curves show the phase transitions of the DODA layer and the DODA−clay hybrid layer from 2D gas to condensed liquid and then to 2D solid during the compression process.[31−33] In the absence of clay, the ∏−*A* isotherm smoothly increases with a lift off area of 164 $Å^2$. When using aqueous clay suspensions as the subphase, the lift-off area of the isotherms increases to higher values, testifying to the adsorption of DODA cations on the

DOI: 10.1021/acsomega.9b01970
ACS Omega 2019, 4, 18100−18107

clay nanoplatelets and thus to the hybridization of the clay platelets with the DODA molecules.[50,51]

The precise control over the packing density of hybrid Langmuir films (DODA−clay) was verified by AFM as shown in Figure 2 (right). Representative AFM images of DODA−clay monolayers deposited at surface pressures of 5, 10, 15, and 20 mN m^{-1} onto Si wafers by the LS technique revealed that the surface coverage scales with the surface pressure. More specifically, the topographic images of DODA−clay monolayers deposited at the lowest surface pressure (Figure 2a) reveal the uniform distribution of isolated clay sheets. When the Langmuir film was compressed to 10 mN m^{-1} (Figure 2b) for deposition, the clay platelets start to contact each other but with still rather large voids between them, and deposition at even higher surface pressures of 15 mN m^{-1} (Figure 2c) and 20 mN m^{-1} (Figure 2d) leads to a denser and more compact packing of the clay sheets. The average thickness of all deposited monolayers of DODA−clay is 1−2 nm as derived from topographical height profile (section analysis) corresponding to the size of single clay layers.[50]

Representative AFM images of the transferred hybrid DODA−clay/SWCNTs-f-OH monolayers are shown in Figure 3, together with the topographic image of SWCNT-f-OH

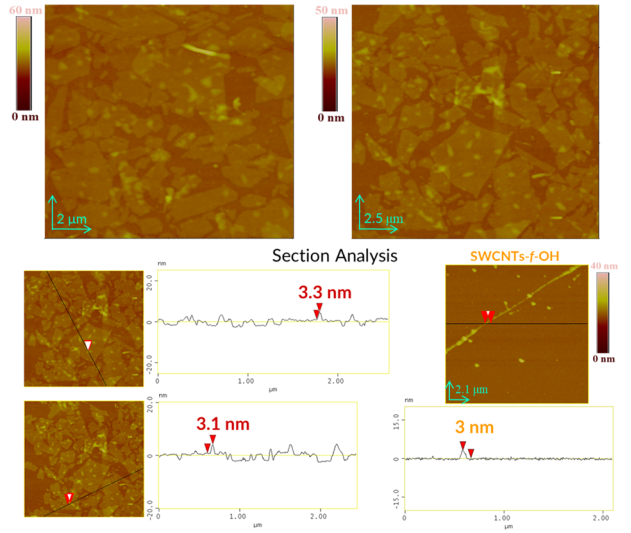

Figure 3. AFM height images (top) and cross-sectional analysis (bottom) of the DODA−clay/SWCNTs-f-OH hybrid monolayer and functionalized SWCNT-f-OH.

deposited by drop-casting from a DMF dispersion. The functionalized SWCNT-f-OH has a diameter of 3 nm, as revealed from the cross-sectional analysis (bottom right panel of Figure 3), suggesting that the addition of phenol groups in the sidewalls of nanotubes was successful and provided well-dispersed and isolated SWCNTs avoiding aggregation due to the covalent addition of −OH groups. On the other hand, the AFM images presented in the top panels of Figure 3 (top) demonstrate that clay nanoplatelets decorated with SWCNTs on the top are successfully transferred to form a layer of (mostly) single platelets with well-defined edges that are almost contacting each other and with small voids between them. The average diameter of the attached SWCNTs on the clay platelets is 3 nm as calculated from the cross-sectional analysis, in agreement with the size of the SWCNTs-f-OH prepared by 1,3-dipolar cycloaddition.

The SWCNT-f-OH attached on the DODA−clay layers are shorter than the pristine SWCNTs because during ultrasonication treatment, the acoustic waves induce a carbon nanotube scission.[52] Moreover, during the Langmuir−Schaefer procedure, the lower-molecular-weight carbon nanotubes float on the surface when the substrate is immersed in the aqueous dispersion of SWCNTs-f-OH to prompt self-assembly, in addition to the heavier (and longer in size) ones that sink and do not interact with the substrate.

Characterization of Clay/CNTs Hybrid Thin Films. X-ray reflectivity (XRR) patterns collected from 40 layers of DODA−clay−DODA and DODA−clay/SWCNTs-f-OH deposited at a surface pressure of 20 mN m^{-1} are presented in Figure 4. The reflectivity curve for DODA−clay−DODA clearly exhibits a prominent (001) Bragg peak at 2.3° (±0.1°), as well as the (002), (003), (004), and (005) Bragg peaks. These features prove that the DODA molecules are grafted on both sides of Kunipia nanoplatelets after the LS procedure, revealing a very well-ordered lamellar structure with a $d_{(001)}$-spacing of 38.4 Å as calculated from the Bragg law and in agreement with our previous results.[50] The XRR of DODA−clay/SWCNTs-f-OH hybrid multilayer on the other hand displays the 001 (n = 1), 002 (n = 2), and 003 (n = 3) diffractions at lower 2θ values, demonstrating that the interlayer distance of the clay nanoplatelets increased due to the incorporation of SWCNTs-f-OH. In more detail, the DODA−clay/SWCNTs-f-OH hybrid multilayer shows a 001 diffraction peak at 2θ = 1.9° (±0.1°), resulting in a d_{001}-spacing of 46.5 Å. This value corresponds to an interlayer space of Δ = 46.5 − 9.6 = 36.9 Å, confirming the presence of SWCNTs-f-OH between the clay platelets. In this case, the Bragg peaks are much broader as a result of the disorder in the hybrid thin film due to the insertion of the nanotubes in the DODA−clay interlayers.

The Raman spectrum of the DODA−clay/SWCNTs-f-OH hybrid multilayer deposited on a Si wafer (40 layers) is shown in Figure 4 (right panel), revealing the characteristic peaks of SWCNTs, namely, the defect-included D band, appear at 1335 cm^{-1} and the two degenerate modes of G band, ω_G^- and ω_G^+, at 1544 and 1590 cm^{-1}, respectively. The small increase of the I_D/I_G ratio (0.22) in the DODA−clay/SWCNTs-f-OH film compared to that of the SWCNTs-f-OH (I_D/I_G = 0.10) is attributed to the shorter length of SWCNTs-f-OH that is deposited between the clay nanoplatelets,[53,54] as was also observed from the AFM study.

The X-ray photoelectron spectroscopy (XPS) analysis is shown in Figure 5; the survey spectrum (top panel) bears the fingerprint of all the characteristic elements expected for the hybrid film. From the detailed spectra, we deduce the following elemental composition: carbon 58.5%, oxygen 29.0%, silicon 11.0%, and nitrogen 1.5%.

The C 1s core level XPS spectrum of DODA−clay/SWCNTs-f-OH is displayed in Figure 5 (central panel) and consists of five components, two peaks at a binding energies of 284.0 and 285.2 eV, which were attributed to the sp^2 and sp^3 hybrid forms of carbon from the SWCNTs as well from the C−C organic chains of DODA molecules representing both of them 76.7% of the whole carbon amount. A fitted peak at 286.2 eV is due to the functionalization of SWCNTs-f-OH, with hydroxyl groups filling 17% of the carbon spectra and attesting the successful attachment of nanotubes with hydroxyl moieties. A very weak photoelectron peak (2.3%) at 288.2 eV may be due to some C−O−C or −COOH groups derived

DOI: 10.1021/acsomega.9b01970
ACS Omega 2019, 4, 18100−18107

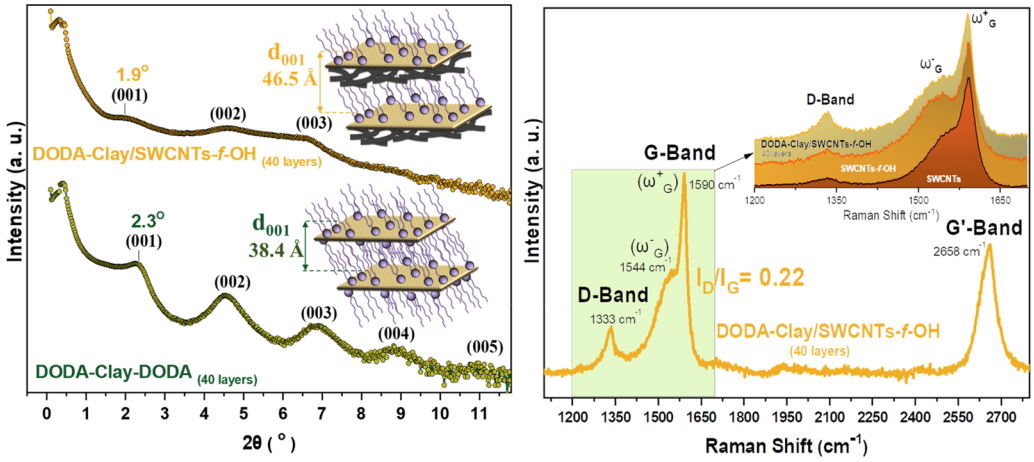

Figure 4. (Left) XRR patterns of DODA−clay−DODA and DODA−clay/SWCNTs-f-OH hybrid multilayers (40 layers). (Right) Raman spectrum of DODA−clay/SWCNTs-f-OH hybrid multilayer (40 layers).

from the impurities absorbed on the nanotubes. Finally, a weak peak at very low binding energies may arise from some type of C−Si bond from the silica substrate or montmorillonite Kunipia impurities.

The N 1s core level region in the photoelectron spectrum (Figure 5, bottom panel) confirms the presence of functionalized SWCNTs between the Kunipia nanosheets[9] (in agreement with XRR results) because the pyrrolidine rings on the functionalized SWCNTs give rise to this spectrum. In fact, the peak at 402.1 eV, accounting for 63.6% of the total N 1s spectral intensity, originates from protonated nitrogen of the pyrrolidine amines of SWCNTs-f-OH, and the nonprotonated pyrrolidine amines of SWCNTs-f-OH are responsible for the contribution at 399.5 eV.

CONCLUSIONS

Hybrid thin films of SWCNTs, functionalized via 1,3-cycloaddition, sandwiched between clay nanoplatelets, were successfully prepared by combining the Langmuir−Schaefer deposition with self-assembly. The efficiency of this approach in terms of coverage and single-layer-level control of the assembly was confirmed by the $\prod$−A isotherms and AFM results. The incorporation of SWCNTs-f-OH in the multilayer structure was confirmed by X-ray photoelectron and Raman spectroscopies. In addition, the XRR measurements revealed that the hybrid multilayer films present a well-ordered lamellar structure with an interlayer space of 36.9 Å. These novel clay pillared with SWCNTs constitutes an ideal synthetic approach for hybrids needed in applications where a high surface area has to be combined with specific functionalities in a well-defined structure, such as materials for energy storage, sensing, catalysis, and nanomedicine. The fabrication of hybrid thin films, combining the properties of 2D materials with carbon nanotubes is a great promise for fabricating novel pillared structures with modified, adjusted, or improved properties.

EXPERIMENTAL SECTION

Materials. A synthetic sodium-saturated montmorillonite Kunipia-F, with a chemical formula $Na_{0.87}[Al_{3.12}Fe(III)_{0.20}Mg_{0.61}Ti_{0.01}](Si_{7.90}Al_{0.10})O_{20}(OH)_4$ and cation-exchange capacity of ∼119 mequiv g^{-1}, was purchased from Kunimine Industries Co. (Japan). Short-length single-walled carbon nanotubes (SWCNTs, ≥90%) were purchased from mkNANO (Canada). Dimethyldioctadecylammonium bromide (DODA, ≥98%), *N*,*N*-dimethylformamide (DMF, ≥99%), 3,4-dihydroxibenzaldehyde (≥97%), acetone, methanol, and ethanol were purchased from Sigma-Aldrich. *N*-Methyl-glycine (≥99%) was purchased from Fluka. Ultrapure deionized water (18.2 MΩ) produced by a Millipore Simplicity system was used throughout. The Si wafers (P/Bor, single side polished, purchased from Si-Mat) were cleaned prior to use by 15 min of ultrasonication in water, acetone, and ethanol. All reagents were of analytical grade and used without further purification.

SWCNTs Functionalization. SWCNTs were functionalized with phenol groups via 1,3-dipolar cycloaddition in a single step.[55−57] More specifically, 25 mg of SWCNTs was suspended in 50 mL of DMF by ultrasonication for 3 min. 250 mg of 3,4-dihydroxibenzaldehyde and 300 mg of N-methyl-glycine were added in the suspension and the mixture was refluxed at 155 °C for 7 days. After the reaction was completed, the functionalized SWCNTs with phenol groups were separated from the byproducts by vacuum filtration using poly(tetrafluoroethylene) filter (from Sigma-Aldrich with a pore size of 0.2 μm and diameter of 47 mm), washed several times with DMF and ethanol, and finally air-dried.

Preparation of Hybrid Clay/CNTs Multilayers. A KSV 2000 Nima Technology Langmuir−Blodgett device was used for the preparation and deposition of clay films at a temperature of 21 ± 0.5 °C. Films were deposited on Si wafers, as depicted in Scheme 1. A 20 ppm clay (Kunipia-F) suspension in ultrapure water (18.2 MΩ Millipore Q-grade) was used as the subphase. To achieve the hybridization of the clay platelets, 100 μL of DODA−solvent mixture (0.2 mg mL^{-1}) was spread onto the water−clay suspension with the help of a microsyringe. After a waiting time of 20 min to allow the evaporation of solvent, the hybrid DODA−clay Langmuir film was compressed at a rate of 5 mm min^{-1} until the chosen stabilization pressure of 20 mN m^{-1} was reached. This pressure was maintained throughout the deposition process. Clay monolayers were transferred onto the hydrophobic substrates by horizontal dipping (Langmuir−Schaefer deposition), with downward and lifting speeds of 10 and 5 mm min^{-1}, respectively. In the final step, the one-side organomodified clay films were lowered in SWCNTs-f-OH (0.2 mg mL^{-1}) dispersion to induce self-assembly.[31−33] Hybrid multilayer thin films were prepared by repeating this procedure 40 times. After

DOI: 10.1021/acsomega.9b01970
ACS Omega 2019, 4, 18100−18107

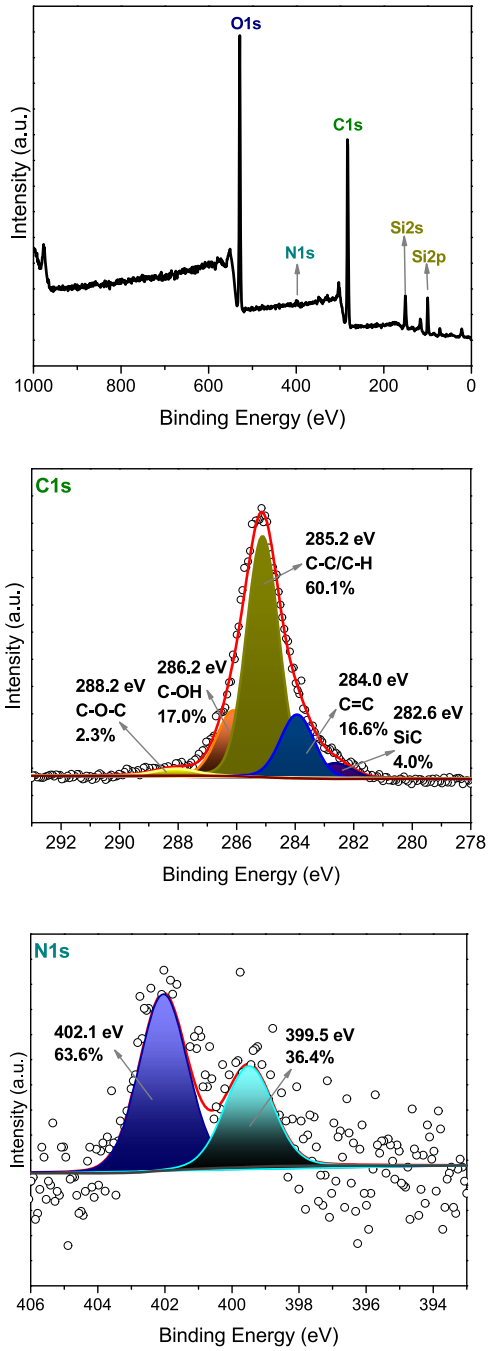

Figure 5. XPS survey (top panel) of C 1s core level (central panel) and N 1s core level (bottom panel) of a DODA−clay/SWCNTs-f-OH hybrid multilayer (40 layers).

each deposition step, the substrates were rinsed several times by dipping into ultrapure water and dried with nitrogen flow to avoid contaminating the Langmuir film in Langmuir−Blodgett trough and/or the SWCNTs-f-OH dispersion. For comparison, an organoclay hybrid multilayer (40 layers) was also fabricated[50] under the same experimental conditions, replacing the SWCNTs-f-OH dispersion in the self-assembly step with DODA surfactant solution in methanol (0.2 mg mL^{-1}) (sample denoted as DODA−clay−DODA).

Characterization Techniques. FTIR spectra in the range 400−4000 cm^{-1} were measured with a PerkinElmer Spectrum GX infrared spectrometer equipped with a deuterated triglycine sulphate detector. Each spectrum was the average of 64 scans, collected with 2 cm^{-1} resolution. Samples were in the form of KBr pellets containing ca. 2 wt % sample. Raman spectra of SWCNTs, SWCNTs-f-OH, and DODA−clay/SWCNTs-f-OH hybrid thin films deposited on the Si wafer were collected with a micro-Raman system RM 1000 RENISHAW using a laser excitation line at 532 nm (laser diode). A 0.5−1 mW laser power was focused on a 1 μm spot to avoid photodecomposition of the hybrid films. Thermal and thermogravimetric analyses (DTA/TGA) were performed using a PerkinElmer Pyris Diamond TG/DTA. Samples of approximately 5 mg were heated in air from 25 to 850 °C at a rate of 5 °C min^{-1}. X-ray reflectivity patterns were collected on a D8 Advance Bruker Diffractometer by using Cu Kα (λ = 1.54 Å) radiation, a molybdenum (Mo) monochromator, and a parallel beam stemming from a Göbel Mirror. They were recorded in the 2θ range from 2 to 12°, with the stepping count of 0.02° and the time between each step set to 2 s. Atomic force microscopy (AFM) images were collected in tapping mode with a Bruker Multimode three-dimensional nanoscope, using a microfabricated silicon cantilever type TAP-300G, with a tip radius <10 nm and a force constant of ∼20−75 N m^{-1}. Pristine SWCNTs-f-OH from DMF dispersion were deposited onto the Si-wafer substrates by drop-casting (∼0.01 mg mL^{-1}). The X-ray photoelectron (XPS) spectra were acquired in a surface analysis ultrahigh-vacuum system (SPECS GmbH) equipped with a twin Al-Mg anode X-ray source and a multichannel hemispherical sector electron analyzer (HSA-Phoibos 100). The energy resolution was set to 1.2 eV and the photoelectron take-off angle was 45° with respect to the surface normal. All binding energies are given ±0.1 eV and were referenced to the SiO_2 core level at 103.5 eV.[58,59] Spectral analysis was performed with the help of a least squares curve-fitting program (WinSpec) developed at the Laboratoire Interdisciplinaire de Spectroscopie Electronique, University of Namur, Belgium, and included a Shirley background subtraction. The profile of the peaks was taken as a convolution of Gaussian and Lorentzian functions. The average uncertainty in the peak intensity determination is 3% for nitrogen and 1% for carbon, silicon, and oxygen.

AUTHOR INFORMATION

Corresponding Authors

*E-mail: antoniokoul@gmail.com (A.K).
*E-mail: dgourni@uoi.gr (D.G).
*E-mail: p.rudolf@rug.nl (P.R).

ORCID

Antonios Kouloumpis: 0000-0002-8738-3141
Panagiota Zygouri: 0000-0002-7137-6633
Konstantinos Spyrou: 0000-0002-2032-8439
Dimitrios Gournis: 0000-0003-4256-8190
Petra Rudolf: 0000-0002-4418-1769

Present Addresses

#Institute of Nanoscience and Nanotechnology, NCSR "Demokritos", Agia Paraskevi- Attikis, 15310 Athens, Greece (T.T.).
⊥Physics Department, University of Ioannina, 45110 Ioannina, Greece (P.S.).

Author Contributions

‖N.C. and A.K. contributed in equal manner to this work.

DOI: 10.1021/acsomega.9b01970
ACS Omega 2019, 4, 18100−18107

Notes

The authors declare no competing financial interest.

■ ACKNOWLEDGMENTS

N.C. and N.K. gratefully acknowledge the IKY Foundation for the financial support: This research was co-financed by Greece and the European Union (European Social Fund, ESF) through the Operational Programme "Human Resources Development, Education and Lifelong Learning" in the context of the project "Strengthening Human Resources Research Potential via Doctorate Research" (MIS-5000432), implemented by the State Scholarships Foundation (IKY). We acknowledge support for this work by the project MIS 5002772, implemented under the Action "Reinforcement of the Research and Innovation Infrastructure", funded by the Operational Programme "Competitiveness, Entrepreneurship and Innovation" (NSRF 2014-2020) and co-financed by Greece and the European Union (European Regional Development Fund).

■ REFERENCES

(1) Fiori, G.; Bonaccorso, F.; Iannaccone, G.; Palacios, T.; Neumaier, D.; Seabaugh, A.; Banerjee, S. K.; Colombo, L. Electronics based on two-dimensional materials. *Nat. Nano* **2014**, *9*, 768−779.

(2) Mousty, C. Sensors and biosensors based on clay-modified electrodes?new trends. *Appl. Clay Sci.* **2004**, *27*, 159−177.

(3) Liu, G.; Jin, W.; Xu, N. Two-Dimensional-Material Membranes: A New Family of High-Performance Separation Membranes. *Angew. Chem., Int. Ed.* **2016**, *55*, 13384−13397.

(4) Sahoo, R.; Pal, A.; Pal, T. 2D materials for renewable energy storage devices: Outlook and challenges. *Chem. Commun.* **2016**, *52*, 13528−13542.

(5) Sun, Z.; Martinez, A.; Wang, F. Optical modulators with 2D layered materials. *Nat. Photonics* **2016**, *10*, 227−238.

(6) Chimene, D.; Alge, D. L.; Gaharwar, A. K. Two-Dimensional Nanomaterials for Biomedical Applications: Emerging Trends and Future Prospects. *Adv. Mater.* **2015**, *27*, 7261−7284.

(7) Gournis, D.; Jankovič, L.; Maccallini, E.; Benne, D.; Rudolf, P.; Colomer, J.-F.; Sooambar, C.; Georgakilas, V.; Prato, M.; Fanti, M.; Zerbetto, F.; Sarova, G. H.; Guldi, D. M. Clay−Fulleropyrrolidine Nanocomposites. *J. Am. Chem. Soc.* **2006**, *128*, 6154−6163.

(8) Georgakilas, V.; Gournis, D.; Bourlinos, A. B.; Karakassides, M. A.; Petridis, D. Clays as a host matrix in the synthesis of organic macrocycles. *Chem. - Eur. J.* **2003**, *9*, 3904−3908.

(9) Georgakilas, V.; Bourlinos, A.; Gournis, D.; Tsoufis, T.; Trapalis, C.; Mateo-Alonso, A.; Prato, M. Multipurpose organically modified carbon nanotubes: from functionalization to nanotube composites. *J. Am. Chem. Soc.* **2008**, *130*, 8733−8740.

(10) Georgakilas, V.; Perman, J. A.; Tucek, J.; Zboril, R. Broad Family of Carbon Nanoallotropes: Classification, Chemistry, and Applications of Fullerenes, Carbon Dots, Nanotubes, Graphene, Nanodiamonds, and Combined Superstructures. *Chem. Rev.* **2015**, *115*, 4744−4822.

(11) Araya-Hermosilla, R.; Pucci, A.; Raffa, P.; Santosa, D.; Pescarmona, P. P.; Gengler, Y. R.; Rudolf, P.; Moreno-Villoslada, I.; Picchioni, F. Electrically-Responsive Reversible Polyketone/MWCNT Network through Diels-Alder Chemistry. *Polymers* **2018**, *10*, 1076.

(12) Tung, T. T.; Pham-Huu, C.; Janowska, I.; Kim, T.; Castro, M.; Feller, J. F. Hybrid Films of Graphene and Carbon Nanotubes for High Performance Chemical and Temperature Sensing Applications. *Small* **2015**, *11*, 3485−3493.

(13) Shi, Y.; Wang, Y.; Wong, J. I.; Tan, A. Y.; Hsu, C. L.; Li, L. J.; Lu, Y. C.; Yang, H. Y. Self-assembly of hierarchical MoSx/CNT nanocomposites (2<x<3): towards high performance anode materials for lithium ion batteries. *Sci. Rep.* **2013**, *3*, No. 2169.

(14) Wang, J.-Z.; Lu, L.; Lotya, M.; Coleman, J. N.; Chou, S.-L.; Liu, H.-K.; Minett, A. I.; Chen, J. Development of MoS2−CNT Composite Thin Film from Layered MoS2 for Lithium Batteries. *Adv. Energy Mater.* **2013**, *3*, 798−805.

(15) Gorkina, A. L.; Tsapenko, A. P.; Gilshteyn, E. P.; Koltsova, T. S.; Larionova, T. V.; Talyzin, A.; Anisimov, A. S.; Anoshkin, I. V.; Kauppinen, E. I.; Tolochko, O. V.; Nasibulin, A. G. Transparent and conductive hybrid graphene/carbon nanotube films. *Carbon* **2016**, *100*, 501−507.

(16) Georgakilas, V.; Tiwari, J. N.; Kemp, K. C.; Perman, J. A.; Bourlinos, A. B.; Kim, K. S.; Zboril, R. Noncovalent Functionalization of Graphene and Graphene Oxide for Energy Materials, Biosensing, Catalytic, and Biomedical Applications. *Chem. Rev.* **2016**, *116*, 5464−5519.

(17) Choi, C. H.; Chung, M. W.; Kwon, H. C.; Chung, J. H.; Woo, S. I. Nitrogen-doped graphene/carbon nanotube self-assembly for efficient oxygen reduction reaction in acid media. *Appl. Catal., B* **2014**, *144*, 760−766.

(18) Núñez, J. D.; Benito, A. M.; Rouziere, S.; Launois, P.; Arenal, R.; Ajayan, P. M.; Maser, W. K. Graphene oxide-carbon nanotube hybrid assemblies: cooperatively strengthened OH[three dots, centered]O[double bond, length as m-dash]C hydrogen bonds and the removal of chemisorbed water. *Chem. Sci.* **2017**, *8*, 4987−4995.

(19) Kim, S. H.; Song, W.; Jung, M. W.; Kang, M.-A.; Kim, K.; Chang, S.-J.; Lee, S. S.; Lim, J.; Hwang, J.; Myung, S.; An, K.-S. Carbon Nanotube and Graphene Hybrid Thin Film for Transparent Electrodes and Field Effect Transistors. *Adv. Mater.* **2014**, *26*, 4247−4252.

(20) Yan, X.; Yang, W.; Shao, Z.; Yang, S.; Liu, X. Graphene/single-walled carbon nanotube hybrids promoting osteogenic differentiation of mesenchymal stem cells by activating p38 signaling pathway. *Int. J. Nanomed.* **2016**, *11*, 5473−5484.

(21) Prashantha, K.; Soulestin, J.; Lacrampe, M. F.; Krawczak, P. Processing and Characterization of Polypropylene Filled with Multiwalled Carbon Nanotube and Clay Hybrid Nanocomposites. *Int. J. Polym. Anal. Charact.* **2014**, *19*, 363−371.

(22) Wang, Z.; Xu, C.; Zhao, Y.; Zhao, D.; Wang, Z.; Li, H.; Lau, K.-t. Fabrication and mechanical properties of exfoliated clay−CNTs/epoxy nanocomposites. *Mater. Sci. Eng., A* **2008**, *490*, 481−487.

(23) Tüzemen, M. Ç.; Salamcı, E.; Avcı, A. Enhancing mechanical properties of bolted carbon/epoxy nanocomposites with carbon nanotube, nanoclay, and hybrid loading. *Composites, Part B* **2017**, *128*, 146−154.

(24) Song, S. H. Synergistic Effect of Clay Platelets and Carbon Nanotubes in Styrene-Butadiene Rubber Nanocomposites. *Macromol. Chem. Phys.* **2016**, *217*, 2617−2625.

(25) Simari, C.; Baglio, V.; Lo Vecchio, C.; Aricò, A. S.; Agostino, R. G.; Coppola, L.; Oliviero Rossi, C.; Nicotera, I. Reduced methanol crossover and enhanced proton transport in nanocomposite membranes based on clay−CNTs hybrid materials for direct methanol fuel cells. *Ionics* **2017**, *23*, 2113−2123.

(26) Al-Saleh, M. H. Clay/carbon nanotube hybrid mixture to reduce the electrical percolation threshold of polymer nanocomposites. *Compos. Sci. Technol.* **2017**, *149*, 34−40.

(27) Egiziano, L.; Lamberti, P.; Spinelli, G.; Tucci, V.; Guadagno, L.; Vertuccio, L. Electrical properties of multiphase composites based on carbon nanotubes and an optimized clay content. *AIP Conf. Proc.* **2016**, *1736*, No. 020146.

(28) Kaffashi, B.; Honarvar, F. M. The effect of nanoclay and MWNT on fire-retardency and mechanical properties of unsaturated polyester resins. *J. Appl. Polym. Sci.* **2012**, *124*, 1154−1159.

(29) Isitman, N. A.; Kaynak, C. Nanoclay and carbon nanotubes as potential synergists of an organophosphorus flame-retardant in poly(methyl methacrylate). *Polym. Degrad. Stab.* **2010**, *95*, 1523−1532.

(30) Hassouna, M. E. M.; ElBably, M. A.; Mohammed, A. N.; Nasser, M. A. G. Assessment of carbon nanotubes and silver nanoparticles loaded clays as adsorbents for removal of bacterial contaminants from water sources. *J. Water Health* **2017**, *15*, 133−144.

(31) Kouloumpis, A.; Dimos, K.; Spyrou, K.; Georgakilas, V.; Rudolf, P.; Gournis, D. A Bottom-Up Approach for the Synthesis of

DOI: 10.1021/acsomega.9b01970
ACS Omega 2019, 4, 18100−18107

Highly Ordered Fullerene-Intercalated Graphene Hybrids. *Front. Mater.* **2015**, *2*, 10.
(32) Dimos, K.; Arcudi, F.; Kouloumpis, A.; Koutselas, I. B.; Rudolf, P.; Gournis, D.; Prato, M. Top-down and bottom-up approaches to transparent, flexible and luminescent nitrogen-doped carbon nanodot-clay hybrid films. *Nanoscale* **2017**, *9*, 10256−10262.
(33) Kouloumpis, A.; Thomou, E.; Chalmpes, N.; Dimos, K.; Spyrou, K.; Bourlinos, A. B.; Koutselas, I.; Gournis, D.; Rudolf, P. Graphene/Carbon Dot Hybrid Thin Films Prepared by a Modified Langmuir−Schaefer Method. *ACS Omega* **2017**, *2*, 2090−2099.
(34) Al-Saleh, M. H. Clay/carbon nanotube hybrid mixture to reduce the electrical percolation threshold of polymer nanocomposites. *Compos. Sci. Technol.* **2017**, *149*, 34−40.
(35) Egiziano, L.; Lamberti, P.; Spinelli, G.; Tucci, V.; Guadagno, L.; Vertuccio, L. In *Electrical Properties of Multiphase Composites Based on Carbon Nanotubes and an Optimized Clay Content*, AIP Conference Proceedings, AIP Publishing, 2016; Vol. 1736, 020146.
(36) Simari, C.; Potsi, G.; Policicchio, A.; Perrotta, I.; Nicotera, I. Clay−Carbon Nanotubes Hybrid Materials for Nanocomposite Membranes: Advantages of Branched Structure for Proton Transport under Low Humidity Conditions in PEMFCs. *J. Phys. Chem. C* **2016**, *120*, 2574−2584.
(37) LeBaron, P. C.; Wang, Z.; Pinnavaia, T. J. Polymer-layered silicate nanocomposites: an overview. *Appl. Clay Sci.* **1999**, *15*, 11−29.
(38) Mittal, V. Polymer Layered Silicate Nanocomposites: A Review. *Materials* **2009**, *2*, 992−1057.
(39) Hassouna, M. E. M.; ElBably, M. A.; Mohammed, A. N.; Nasser, M. A. G. Assessment of carbon nanotubes and silver nanoparticles loaded clays as adsorbents for removal of bacterial contaminants from water sources. *J. Water Health* **2017**, *15*, 133−144.
(40) Yao, Z.; Braidy, N.; Botton, G. A.; Adronov, A. Polymerization from the surface of single-walled carbon nanotubes - preparation and characterization of nanocomposites. *J. Am. Chem. Soc.* **2003**, *125*, 16015−16024.
(41) Dyke, C. A.; Tour, J. M. Covalent Functionalization of Single-Walled Carbon Nanotubes for Materials Applications. *J. Phys. Chem. A* **2004**, *108*, 11151−11159.
(42) Jorio, A.; Souza Filho, A. G. Raman Studies of Carbon Nanostructures. *Annu. Rev. Mater. Res.* **2016**, *46*, 357−382.
(43) Lian, Y.; Maeda, Y.; Wakahara, T.; Nakahodo, T.; Akasaka, T.; Kazaoui, S.; Minami, N.; Shimizu, T.; Tokumoto, H. Spectroscopic study on the centrifugal fractionation of soluble single-walled carbon nanotubes. *Carbon* **2005**, *43*, 2750−2759.
(44) Arepalli, S.; Nikolaev, P.; Gorelik, O.; Hadjiev, V. G.; Holmes, W.; Files, B.; Yowell, L. Protocol for the characterization of single-wall carbon nanotube material quality. *Carbon* **2004**, *42*, 1783−1791.
(45) Filho, A. G. S.; Jorio, A.; Ge, G. S.; Dresselhaus, G.; Saito, R.; Dresselhaus, M. S. Raman spectroscopy for probing chemically/physically induced phenomena in carbon nanotubes. *Nanotechnology* **2003**, *14*, 1130.
(46) Ago, H.; Nakamura, K.; Uehara, N.; Tsuji, M. Roles of Metal−Support Interaction in Growth of Single- and Double-Walled Carbon Nanotubes Studied with Diameter-Controlled Iron Particles Supported on MgO. *J. Phys. Chem. B* **2004**, *108*, 18908−18915.
(47) Ci, L.; Zhou, Z.; Yan, X.; Liu, D.; Yuan, H.; Song, L.; Wang, J.; Gao, Y.; Zhou, J.; Zhou, W.; Wang, G.; Xie, S. Raman Characterization and Tunable Growth of Double-Wall Carbon Nanotubes. *J. Phys. Chem. B* **2003**, *107*, 8760−8764.
(48) Lyu, S. C.; Liu, B. C.; Lee, C. J.; Kang, H. K.; Yang, C.-W.; Park, C. Y. High-Quality Double-Walled Carbon Nanotubes Produced by Catalytic Decomposition of Benzene. *Chem. Mater.* **2003**, *15*, 3951−3954.
(49) Colomer, J. F.; Stephan, C.; Lefrant, S.; Van Tendeloo, G.; Willems, I.; Kónya, Z.; Fonseca, A.; Laurent, C.; Nagy, J. B. Large-scale synthesis of single-wall carbon nanotubes by catalytic chemical vapor deposition (CCVD) method. *Chem. Phys. Lett.* **2000**, *317*, 83−89.
(50) Toma, L. M.; Gengler, R. Y.; Prinsen, E. B.; Gournis, D.; Rudolf, P. A Langmuir-Schaefer approach for the synthesis of highly ordered organoclay thin films. *Phys. Chem. Chem. Phys.* **2010**, *12*, 12188−12197.
(51) Gengler, R. Y.; Toma, L. M.; Pardo, E.; Lloret, F.; Ke, X.; Van Tendeloo, G.; Gournis, D.; Rudolf, P. Prussian blue analogues of reduced dimensionality. *Small* **2012**, *8*, 2532−2540.
(52) Ji, M.; Daniels, B.; Shieh, A.; Modarelli, D. A.; Parquette, J. R. Controlling the length of self-assembled nanotubes by sonication followed by polymer wrapping. *Chem. Commun.* **2017**, *53*, 12806−12809.
(53) Chou, S. G.; Son, H.; Kong, J.; Jorio, A.; Saito, R.; Zheng, M.; Dresselhaus, G.; Dresselhaus, M. S. Length characterization of DNA-wrapped carbon nanotubes using Raman spectroscopy. *Appl. Phys. Lett.* **2007**, *90*, No. 131109.
(54) Fagan, J. A.; Simpson, J. R.; Bauer, B. J.; De Paoli Lacerda, S. H.; Becker, M. L.; Chun, J.; Migler, K. B.; Hight Walker, A. R.; Hobbie, E. K. Length-Dependent Optical Effects in Single-Wall Carbon Nanotubes. *J. Am. Chem. Soc.* **2007**, *129*, 10607−10612.
(55) Georgakilas, V.; Kordatos, K.; Prato, M.; Guldi, D. M.; Holzinger, M.; Hirsch, A. Organic functionalization of carbon nanotubes. *J. Am. Chem. Soc.* **2002**, *124*, 760−761.
(56) Georgakilas, V.; Bourlinos, A. B.; Zboril, R.; Steriotis, T. A.; Dallas, P.; Stubos, A. K.; Trapalis, C. Organic functionalisation of graphenes. *Chem. Commun.* **2010**, *46*, 1766−1768.
(57) Georgakilas, V. Chemical functionalization of ultrathin carbon nanosheets. *Fullerenes, Nanotubes, Carbon Nanostruct.* **2010**, *18*, 87−95.
(58) Naumkin, A. V.; Kraut-Vass, A.; Gaarenstroom, S. W.; Powell, C. J. *NIST X-ray Photoelectron Spectroscopy Database, NIST Standard Reference Database 20*, version 4.1; US Department of Commerce: Washington, 2012.
(59) Hantsche, H. High resolution XPS of organic polymers, the scienta ESCA300 database. By G. Beamson and D. Briggs, Wiley, Chichester 1992, 295 pp., hardcover, £ 65.00, ISBN 0-471-93592-1. *Adv. Mater.* **1993**, *5*, 778.

DOI: 10.1021/acsomega.9b01970
ACS Omega 2019, 4, 18100−18107